Modeling the crystallization of gold nanoclusters—the effect of the potential energy function

2009 J. Phys.: Condens. Matter 21 144207

(http://iopscience.iop.org/0953-8984/21/14/144207)

IOP Publishing Journal of Physics: Condensed Matter

J. Phys.: Condens. Matter **21** (2009) 144207 (8pp) doi:10.1088/0953-8984/21/14/144207

Modeling the crystallization of gold nanoclusters—the effect of the potential energy function

Yu Hang Chui[1], George Opletal[2], Ian K Snook[2] and Salvy P Russo[2,3]

[1] Institut fuer Physik, Universitaet Mainz, Staudinger Weg 7, D-55099 Mainz, Germany
[2] Applied Physics, School of Applied Sciences, RMIT University, GPO Box 2476V, Melbourne, VIC, 3001, Australia

E-mail: salvy.russo@rmit.edu.au

Received 3 September 2008, in final form 28 October 2008
Published 18 March 2009
Online at stacks.iop.org/JPhysCM/21/144207

Abstract

The crystallization dynamics of 5083 atom gold nanoclusters, which were quenched from the melt, were studied by molecular dynamics (MD) using the EAM 'Glue' and 'Force-matched' potentials to compare and contrast how the crystallization dynamics is affected by these potential energy functions. MD simulations from each potential showed the formation of gold nanoclusters of icosahedral morphology during the quenching process, which is in good agreement with the experimental studies of gold nanoclusters formed under vacuum. The effect of the potential on the evolution of cluster (surface and interior) morphology during the crystallization process is discussed.

(Some figures in this article are in colour only in the electronic version)

1. Introduction

Studies of nano-scaled gold particles have been one of the active areas of material science research, as tiny gold particles have a wide range of potential applications in electronics, medicine and catalysis [1].

Critical parameters that affect the electronic, optical, and catalytic properties of these nanoclusters are their size and shape [2–6] and these morphological parameters are in turn dependent on how the nanoclusters crystallize. Although there has been good progress made in the synthesis of gold nanostructures, controlled fabrication of structures with specific optical or electronic properties still cannot be routinely achieved. Therefore, understanding the mechanisms underlying the crystallization of gold nanoclusters is important if one hopes to control their size and morphology and therefore their properties.

In terms of shape, the first systematic investigation of gold nanoparticle motifs was undertaken by Ino [7], who calculated the free energy of various shaped nanocrystals and concluded that those of the Mackay icosahedron (m-Ih) motif are likely to be the energetically most favored below ∼10 nm in diameter. Recently there have been a number of studies investigating, as the function of nanocluster size, the relative stability of various structural motifs of nanocrystalline gold including; 'Mackay icosahedra' (m-Ih), 'Marks decahedra' (m-Dh), 'truncated octahedra' (TOh) and FCC [8–11].

Theoretical/computational studies on crystallization of Au nanoclusters by freezing have been conducted by Chui *et al* [12, 13, 21], Rossi and Ferrando [14], Kuo and Clancy [15], Shim *et al* [16], Nam *et al* [17] and Wang *et al* [18]. Apart from the study of Rossi (who used a Gupta potential), all these studies used an embedded atom method (EAM) type potential such as the EAM (Glue) [19] or modified EAM potential [20]. Irrespective of the potential used, the formation of icosahedral-like clusters resulting from quenching from the liquid state is common to all these studies.

Rossi [14] identified several different structures resulting from freezing of gold clusters and found that formation of icosahedra is more favorable at fast quenching rates, while the occurrence of decahedral and FCC structures increased at slower cooling rates. The molecular dynamics (MD)

[3] Author to whom any correspondence should be addressed.

studies of Shim [16], Wang [18] and Chui *et al* [12, 13] all showed that defected icosahedral particles are formed from quenching of gold particles from the melt over a range of nanocluster sizes. The study of Chui *et al* [13] also showed by quantitative structural analysis, that nanocluster crystallization appears to initiate at the surface and proceed into the core. This observation was previously suggested by Nam *et al* [17] and has been recently been supported by the study of Sutter and Sutter [22] who provide experimental evidence for this occurring.

Possible explanations for the prevalence of icosahedral nanoclusters resulting from quenching from the molten state have been offered by Barnard *et al* [11] and Kuo [15].

Grochola *et al* has also conducted a number of theoretical MD studies on the formation of gold nanoclusters using a new 'Force-matched' embedded atom potential [23]. These studies include, prediction of the relative stability of differing gold nanocluster morphologies [10], investigating the mechanism underlying the formation of 'pancake' decahedral nanoclusters [24] and the prediction of the kinetic mechanism for the formation of nanorod growth [25] in a two surfactant bath.

Therefore the purpose of this paper is to compare and contrast the predictions of cluster crystallization and morphology (resulting from quenching) using the EAM Glue potential, which have been used in previous studies of gold nanocluster crystallization [12, 13, 18], with the Force-matched potential of Grochola [23] with a view to identifying common features in the crystallization dynamics and the bulk and surface morphology.

2. Modeling and simulation method

2.1. Glue and force-matched potentials

The most widely used potential model for modeling metal systems is the embedded atom method (EAM) potential.

In the EAM description, the total energy is given by

$$E_{\text{tot}} = \sum_i F_i(\rho_h, i) + \tfrac{1}{2} \sum_{\substack{i,j \\ i \neq j}} \phi_{ij}(R_{ij}), \qquad (1)$$

where Φ_{ij} is the pair potential and F_i is embedding term which models the electronic interaction between gold atoms. The Glue and Force-matched potentials are both based on the EAM formalism with the only difference being the method for finding the parameters used in the potential. In the case of the Glue potential, Ercolessi *et al* [19] obtained the parameters by fitting to experimental bulk and surface properties. This potential gives a good description of bulk properties and is able to describe the (100) semi-hexagonal reconstruction on gold surfaces as well as other surface properties, which were not accurately given in the original EAM description of gold [26]. The Force-matched potential was fitted using an improved force-matched methodology, which includes high-temperature solid lattice constants and liquid densities [23]. This potential gives better overall agreement with experimental bulk properties and surface energies, compared to the original EAM [26] and Glue potentials [19].

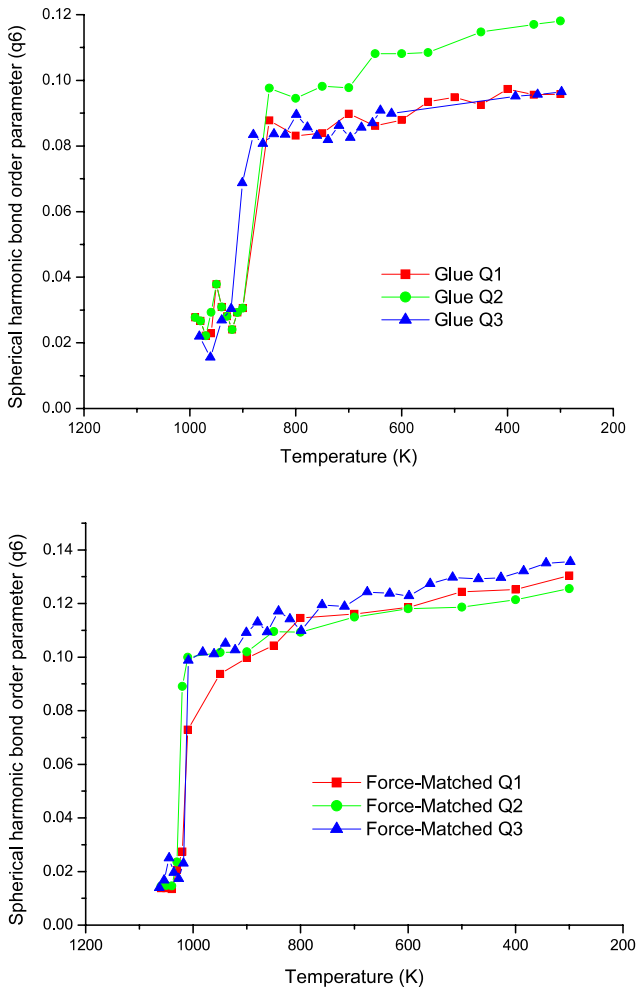

Figure 1. The variation of the bond order parameter ($q6$) during the quenching process of the gold nanoclusters modeled by the Glue potential (upper), and the Force-matched potential (lower).

2.2. Simulation procedure

Perfect 5083 atom 'Mackay' icosahedra were heated to 1400 K using MD until they achieved liquid-like equilibrium. An MD simulation time of 1.5 ns was required to achieve this state. These clusters were then quenched down to a temperature of 298 K using three different quenching rates $Q1$ (2×10^4 time steps per 10 K), $Q2$ (2×10^4 time steps per 5 K) and $Q3$ (2×10^4 time steps per 3 K). At selected temperatures during the quenching process (which corresponded to every 10, 5 and 3 K for $Q1$, $Q2$ and $Q3$ respectively) we also followed the time evolution of the crystallization process at those temperatures by performing an *NVT*-MD. The data points in figure 1 indicate the temperatures at which we followed this time evolution for each of the quench rates $Q1$, $Q2$ and $Q3$. During each *NVT*-MD time evolution of the crystallization simulation, the cluster was allowed to re-equilibrate at that temperature for 0.2 ns, after which time the structure was analyzed using our analysis methods discussed below. All MD simulations used a time step of 5 fs.

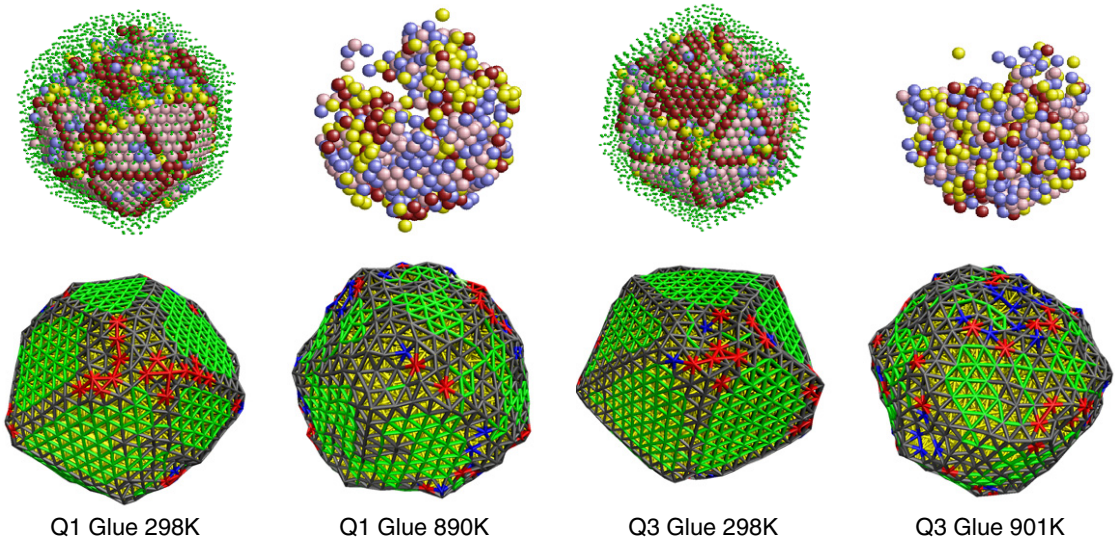

Figure 2. The Au nanoparticles with quench rate $Q1$ (left half) and $Q3$ (right half) modeled by the Glue potential. Top row figures give a snapshot of the core structure and the corresponding surface structure of the nanoclusters is given in the bottom row. The temperatures of 890 K and 901 K represent the approximate temperatures for the beginning of crystallization for the $Q1$ and $Q3$ quench rates, respectively. The coloring scheme for both the core and surface atoms is defined in section 3.2.

2.3. Structural characterization

In considering the morphological structure of nanoclusters, we believe it is difficult to base any conclusion on visual inspection of the cluster. In addition, common theoretical methods used to probe the structure of formed clusters, such as the radial distribution function (RDF) and bond angle distribution function (BADF) can only provide a spatial average of the local environment of individual atoms. Therefore we have developed (and describe elsewhere [13, 21]), a quantitative analysis method of local ordering of atoms in the core and surface of a cluster. The local structural environment of each core atom in a cluster is classified using a scheme based on planar graphs and shortest-path (SP) ring analysis, while the scheme used to determine the morphology of surface atoms is based on surface curvature, bond angles and atom coordination as described below.

The surface characterization was performed by first determining which atoms in the cluster are surface atoms. This was determined by filling the system with a cubic lattice of pseudo-atoms (labeled p-atoms), removing any p-atoms that overlap real atoms and then determining if any real atoms are neighbors to these p-atoms. Atoms having any neighboring p-atoms are labeled surface atoms. This procedure was repeated over a shifting lattice of p-atoms to ensure that proper sampling picks up all the surface atoms.

After the determination of the surface layer, for each of the surface atoms, the surface coordination (number of bonds surface atoms have with other neighboring surface atoms), local curvature and surface bond angles were calculated. The local curvature for a particular atom was calculated by the triple scalar product between the displacement vectors to the nearest neighbors i, j and k.

For perfect surfaces, (111) like atoms have zero curvature, six nearest surface neighbors and an average angle of 60° while (100) like atoms have zero curvature, four nearest surface neighbors and an average bond angle of 90°. For non-ideal, thermally fluctuating systems, a bond angle and curvature tolerance range is used to characterize these surface packing environments. To highlight the (111) surfaces in this study, the bond angle range used was 45°–60° with six nearest neighbors and a curvature range of 82°–98°.

3. Result and discussion

3.1. Analysis based on the q6 parameter

Figure 1 shows the calculated value of the $q6$ order parameter as a function of temperature during the quenching of a 5083 atom gold nanocluster from 1400 to 298 K. The $q6$ values for the three quench rates using the Glue (top) and Force-matched (bottom) EAM potentials are given. The $q6$ order parameter has been showed to be a very good indicator of cluster crystallinity [27–29] and a sharp transition in $q6$ indicates the temperature region where significant structural ordering (freezing) begins to occur. Using the Glue potential this occurs between 922 and 880 K while for the 'Force-matched' potential it is between 1018 and 1009 K.

Figure 1 suggests that the freezing temperature and the cluster ordering are more dependent on quench rate for the Glue potential than it is for the Force-matched. In addition, at all quench rates, the cluster becomes more ordered at 298 K if quenched using the Force-matched potential.

3.2. Visualization using planar graph sequencing

Figure 2 shows the local structural ordering in the core atoms (top row) and surface atoms (bottom row) of a gold nanocluster at high temperature and at 298 K as modeled by the Glue potential. Figure 3 gives the corresponding results using the Force-matched potential. The following color scheme was used to classify the core atoms in the nanocluster: FCC (pink), defected FCC (blue), HCP (yellow) and defected HCP (red).

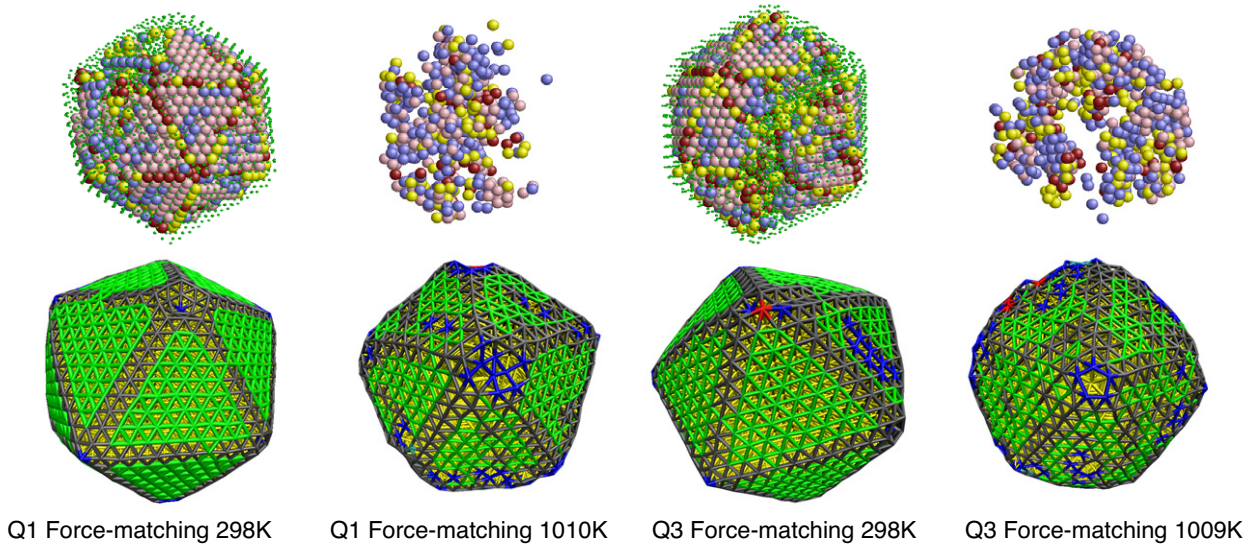

Figure 3. The Au nanoparticles with quench rate $Q1$ (left half) and $Q3$ (right half) modeled by the Force-matched potential. Top row figures give a snapshot of the core structure and the corresponding surface structure of the nanoclusters is given in the bottom row. The temperatures of 1010 K and 1009 K represent the approximate temperatures for the beginning of crystallization for the $Q1$ and $Q3$ quench rates, respectively. The coloring scheme for both the core and surface atoms is defined in section 3.2.

Table 1. Surface analysis of the nanoclusters.

	Glue $Q1$	Glue $Q2$	Glue $Q3$	FM $Q1$	FM $Q2$	FM $Q3$
Number of surface atoms	1354	1371	1371	1257	1259	1261
Surface coordination						
1	0	0	0	0	0	0
2	0	0	0	1	0	0
3	0	0	0	1	0	0
4	1	0	1	6	2	0
5	39	31	35	45	62	50
6	1249	1247	1274	1194	1189	1203
7	65	93	59	10	6	8
8	0	0	2	0	0	0
9	0	0	0	0	0	0
10	0	0	0	0	0	0
Surface classification						
(111)	933	910	976	1090	1103	1121
(100)	0	0	0	0	0	0
(110)	0	0	0	0	0	0
Number of step atoms	263	312	208	105	90	91

Core atoms which have a highly disordered or amorphous local structural environment are white and therefore not shown. The green atoms in the top row figures represent surface atoms and have no structural significance. The color scheme used to classify the surface atoms and their bonds figures 2 and 3 (bottom row) is surface atoms with 7 nearest surface neighbors (NSN) (red), 6 NSN (gray), 5 NSN (dark blue), 4 NSN (light blue). Atoms and bonds which lie on a (111) surface plane are designated green. As indicated earlier, these surface classifications are based on a scheme which determines the surface atoms local curvature, bond angle and coordination within a cutoff distance.

The figures show that both potentials predict similar cluster morphology at 298 K, which is a defected icosahedral morphology. Perhaps the greatest contrast is that the Force-matched potential favors the formation of extended (111) facets on the nanocluster surface without surface reconstruction, whereas surface reconstruction is evident in the clusters modeled using the Glue potential. In addition, sharp edges between two adjacent (111) facets and a vertex of five-fold symmetry were often observed in the nanoclusters modeled by the Force-matched potential.

In a previous study [13] we found using the Glue potential predicted a surface induced cluster crystallization, with core crystallization beginning below one (111) facet of the five-fold symmetrical surface and then proceeding to the other core regions. As the crystallization proceeded, new FCC core fragments were formed adjacent to the large existing FCC

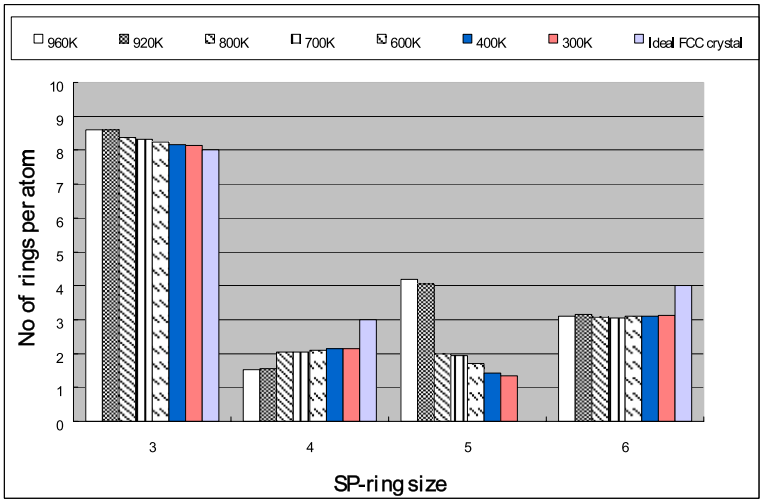

Q1

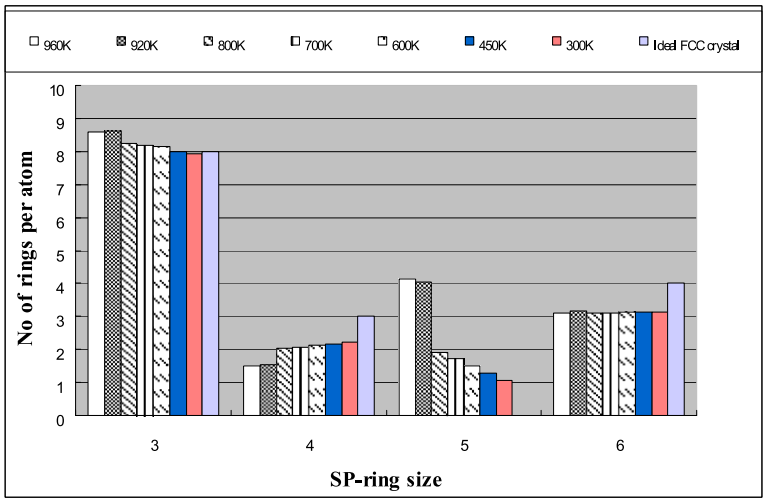

Q2

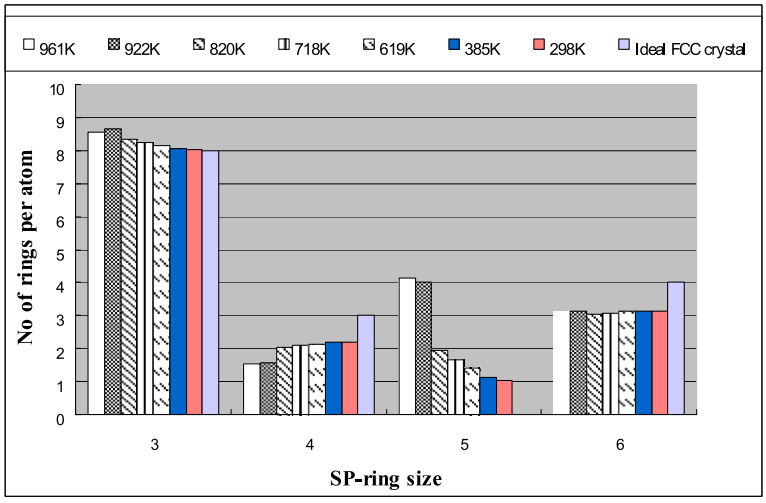

Q3

Figure 4. Shortest-path (SP) ring statistics with the quenching rates $Q1$ (top), $Q2$ (middle) and $Q3$ (bottom) as modeled by the Glue potential.

fragment. As a result, one single FCC crystalline core grew inside the nanocluster during the cooling process.

Although not evident in figures 2 and 3, results for the nanoclusters modeled by Force-matched potential, suggest that during crystallization several separated aggregates of local FCC structure are formed in the amorphous region just below the extended crystalline surface, in the early stage of crystallization. The appearance of multiple FCC regions as opposed to the single region seen with the Glue potential is most likely due to the much less disordered surface produced

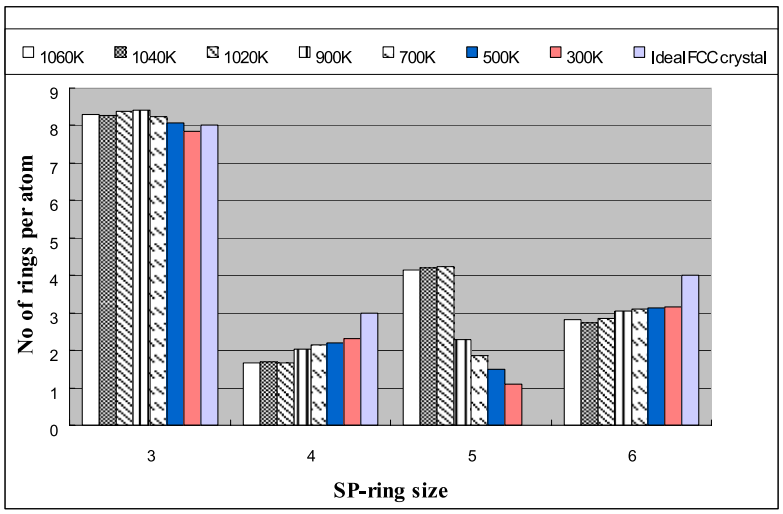

Figure 5. Shortest-path (SP) ring statistics with the quenching rates $Q1$ (top), $Q2$ (middle) and $Q3$ (bottom) as modeled by the Force-matched potential.

by the Force-matched potential. Table 1 gives an analysis of the surface morphology of the nanoclusters based on our surface atom classification scheme.

3.3. Shortest-path (SP) and planar graph ring statistics

Figures 4 and 5 show the shortest-path (SP) ring statistics for the core atoms in the gold nanocluster as modeled by Glue

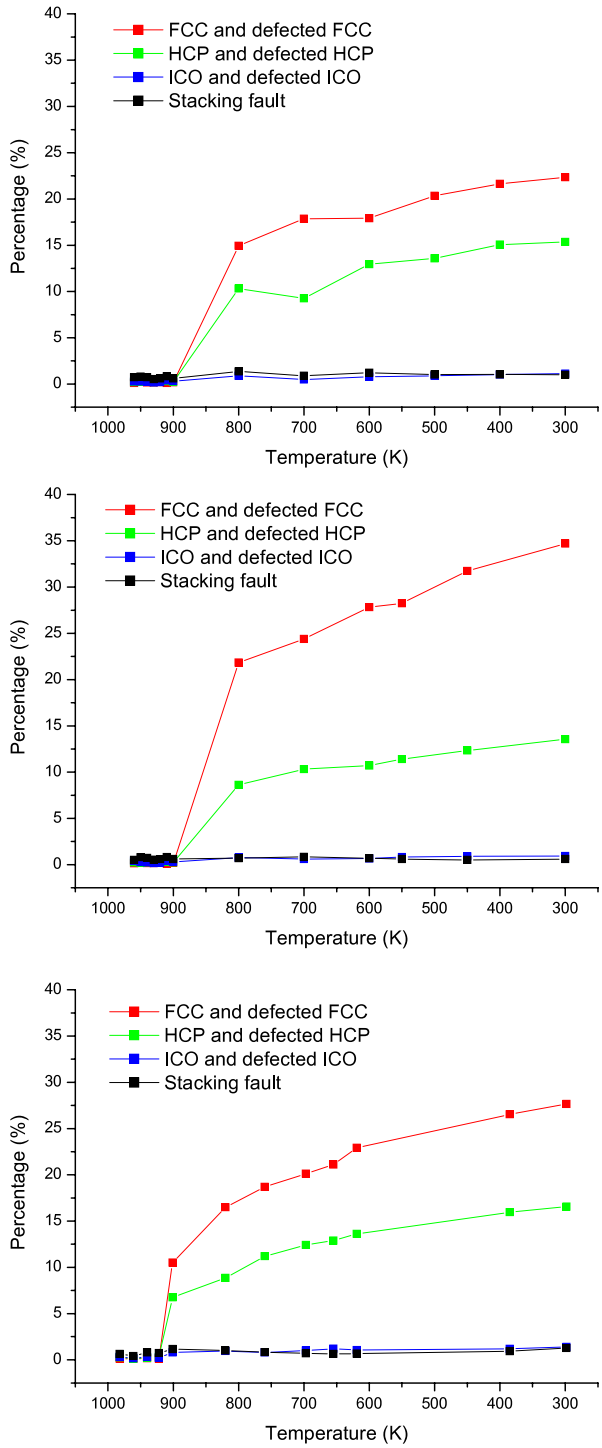

Figure 6. The percentage variation of FCC, HCP, ICO and stacking fault content with the quenching rates $Q1$ (top), $Q2$ (middle), $Q3$ (bottom) modeled by the Glue potential during the quench.

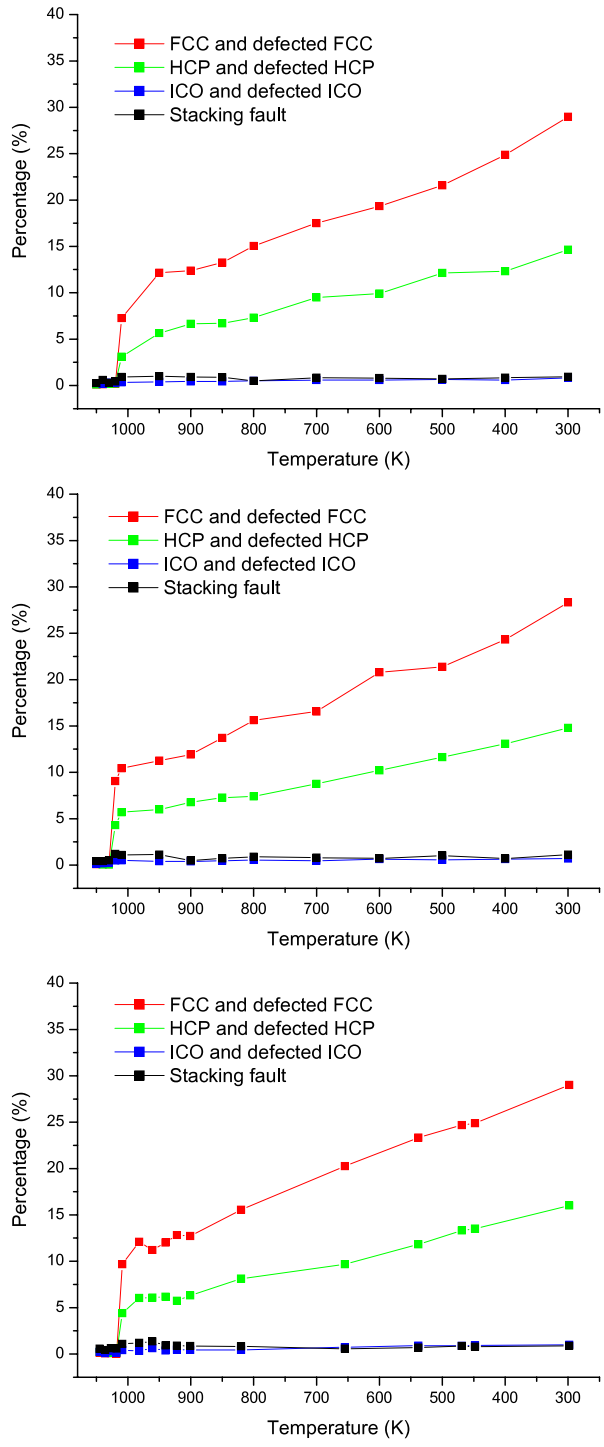

Figure 7. The percentage variation of FCC, HCP, ICO and stacking fault content with the quenching rates $Q1$ (top), $Q2$ (middle), $Q3$ (bottom) modeled by the Force-matched potential during the quench.

(figure 4) and Force-matched (figure 5) potentials respectively. A discussion of how SP-ring statistics and planar graphs relate to structure is given in a previous work [13, 21]. Both potentials show similar trends for all SP-ring sizes. At all quench rates, as the temperature decreases we note the gradual increase of 4-membered rings and a sharp decrease of 5-membered rings, which indicates the crystallization inside the core of the gold nanoclusters. It is also interesting to note that there is almost no change in the number of 6-membered rings during quenching as modeled by the Glue potentials while the Force-matched potential does predict a gradual increase with decreasing temperature.

Figures 6 and 7 show the planar graph ring sequencing statistics for core atoms with FCC, defected FCC, HCP,

defected HCP, ICO and defected ICO local structure. The figures show that with the Glue potential (figure 6), the quench rate significantly effects core local structure at 298 K, while for the Force-matched potential (figure 7) the relative percentages of FCC, HCP and ICO classified core atoms remain approximately the same at 298 K independent of quench rate.

4. Conclusion

To conclude, although there are differences in the details of the surface and core structures predicted by the two atomistic potentials in this study of a 5083 atom gold nanocluster the broad features of the freezing process are very similar. For example both potentials predicted a defected icosahedral-like morphology. The cluster morphology is dependent on quench rate for the Glue potential but less so for the Force-matched potential. For both potentials there is strong evidence showing that crystallization of the surface precedes that of the core.

Acknowledgments

This project was supported by the Australian Partnership for Advanced Computing APAC and the Victorian Partnership for Advanced Computing VPAC. One of the authors YHC would also like to thank RMIT University for its financial assistance.

References

[1] Daniel M C and Astruc D 2004 *Chem. Rev.* **104** 293
Xiao Y, Patolsky F, Katz E, Hainfeld J F and Willner I 2003 *Science* **299** 1877
[2] Pérez-Juste J, Pastoriza-Santos I, Liz-Marzán L M and Mulvaney P 2005 *Coord. Chem. Rev* **249** 1870
[3] Sau T K and Murphy C J 2004 *J. Am. Chem. Soc.* **126** 8648
[4] Hu J, Zhang Y, Liu B, Liu J, Zhou H, Xu Y, Jiang Y, Yang Z and Tian Z-Q 2004 *J. Am. Chem. Soc.* **126** 9470
[5] Sanchez-Castillo M A, Couto C, Kim W B and Dumesic J A 2004 *Angew. Chem. Int. Edn* **43** 1140
[6] Hao E, Bailey R C, Schatz G C, Hupp J T and Li S 2004 *Nano Lett.* **4** 327
[7] Ino S J 1969 *J. Phys. Soc. Japan* **27** 941
[8] Cleveland C L, Landman U, Schaaff T G, Shafigullin M N, Stephens P W and Whetten R L 1997 *Phys. Rev. Lett.* **79** 1873
[9] Cleveland C, Luedtke W D and Landman U 1998 *Phys. Rev. Lett.* **81** 2036
Cleveland C, Luedtke W D and Landman U 1999 *Phys. Rev.* B **60** 5065
[10] Grochola G, Snook I K and Russo S P 2007 *J. Chem. Phys.* **127** 224704
[11] Barnard A S, Opletal G, Snook I K and Russo S P 2008 *J. Phys. Chem.* C **112** 14848
[12] Chui Y H, Snook I K and Russo S P 2007 *Phys. Rev.* B **75** 033404
[13] Chui Y H, Snook I K and Russo S P 2007 *Phys. Rev.* B **76** 195427
[14] Rossi G and Ferrando R 2007 *Nanotechnology* **18** 225706
[15] Kuo C L and Clancy P 2005 *J. Phys. Chem.* B **109** 13743
[16] Shim J-H, Lee S-C, Lee B-J, Suh J-Y and Cho Y W 2003 *J. Cryst. Growth* **250** 558
[17] Nam H S, Hwang N M, Yu B D and Yoon J K 2002 *Phys. Rev. Lett.* **89** 275502
[18] Wang Y, Teitel S and Dellago C 2005 *J. Chem. Phys.* **122** 214722
[19] Ercolessi F, Tosatti E and Parrinello M 1986 *Phys. Rev. Lett.* **57** 719
Ercolessi F, Parrinello M and Tosatti E 1988 *Phil. Mag.* A **58** 213
[20] Baskes M I 1992 *Phys. Rev.* B **46** 2727
[21] Chui Y H, Rees R J, Snook I K, O'Malley B and Russo S P 2006 *J. Chem. Phys.* **125** 114703
[22] Sutter P W and Sutter E A 2007 *Nat. Mater.* **6** 363
[23] Grochola G, Russo S P and Snook I K 2005 *J. Chem. Phys.* **123** 204719
[24] Grochola G, Russo S P and Snook I K 2007 *J. Chem. Phys.* **127** 224705
[25] Grochola G, Snook I K and Russo S P 2007 *J. Chem. Phys.* **127** 194707
[26] Daw M S and Baskes M I 1984 *Phys. Rev.* B **29** 6443
Daw M S and Baskes M I 1983 *Phys. Rev. Lett.* **50** 1285
[27] O'Malley B and Snook I K 2003 *Phys. Rev. Lett.* **90** 085702
O'Malley B and Snook I K 2005 *J. Chem. Phys.* **123** 054511
[28] Fransblau D S 1991 *Phys. Rev.* B **44** 4925
[29] van Duijneveldt J D and Frenkel D 1992 *J. Chem. Phys.* **96** 4655